Nanostructures

International Edition: DOI: 10.1002/anie.201500267
German Edition: DOI: 10.1002/ange.201500267

Formation of Nickel Sulfide Nanoframes from Metal–Organic Frameworks with Enhanced Pseudocapacitive and Electrocatalytic Properties

*Xin-Yao Yu, Le Yu, Hao Bin Wu, and Xiong Wen (David) Lou**

Abstract: *Nanoframe-like hollow structures with unique three-dimensional (3D) open architecture hold great promise for various applications. Current research efforts mainly focus on frame-like noble metals and metal oxides. However, metal sulfides with frame-like nanostructures have been rarely reported. Starting from metal–organic frameworks (MOFs), we demonstrate a novel structure-induced anisotropic chemical etching/anion exchange method to transform Ni-Co Prussian blue analogue (PBA) nanocubes into NiS nanoframes with tunable size. The reaction between Ni-Co PBA nanocube templates and Na_2S in solution leads to the formation of well-defined NiS nanoframes. The different reactivity between the edges and the plane surface of the Ni-Co PBA nanocubes is found to be the key factor for the formation of NiS nanoframes. Benefitting from their structural merits including 3D open structure, small size of primary nanoparticles, high specific surface area, and good structural robustness, the as-derived NiS nanoframes manifest excellent electrochemical performance for electrochemical capacitors and hydrogen evolution reaction in alkaline electrolyte.*

Hollow micro/nanostructured materials have attracted increasing interest due to their unique structures, intriguing properties that differ from their solid counterparts, and widespread applications in many areas, such as energy storage and conversion, electrocatalysts, chemical sensors, and so on.[1–6] Among the reported hollow nanostructures, nanoframe-like structures with open three-dimensional (3D) architectures have provoked ever-increasing attention.[7–15] In recent years, hollow frame-like noble metal and metal oxides nanostructures have been successfully fabricated by using many advanced methods.[16–20] For example, we have reported one-pot synthesis of cubic $PtCu_3$ nanoframes with enhanced electrocatalytic activity for the methanol oxidation reaction.[11] Most recently, Pt_3Ni nanoframes have been synthesized and exhibit enhanced activity for the oxygen reduction reaction arising from their 3D molecular accessibility.[19] Huang and co-workers reported the fabrication of truncated rhombic dodecahedral Cu_2O nanoframes through particle aggregation and acidic etching.[8] Despite these great advances, previous reports mostly focus on noble metals and metal oxides. To the best of our knowledge, nanoframe-like metal sulfides are rarely reported, mainly due to the difficulty in finding proper templates or effective synthetic methods. Considering the unique physical and chemical properties and wide applications of nanostructured metal sulfides, it is highly demanded to develop feasible methods for synthesis of hollow metal sulfides with well-defined frame-like nanostructures.

As a class of crystalline metal–organic frameworks (MOFs), Prussian blue analogues (PBA) with the formula of $M^{II}_3[M^{III}(CN)_6]_2{\cdot}nH_2O$ (M = Fe, Ni, Co, etc.) can be synthesized with uniform sizes, various compositions, diverse morphologies and architectures.[21–23] Due to their special thermal properties and unique reactivity, nanostructured PBA materials have been extensively investigated as precursors/templates to develop new functional nanomaterials with hollow or porous structures.[21,24–28] We have reported the facile synthesis of hollow metal oxide/hydroxide microboxes through annealing treatment or chemical reaction between PB and NaOH solution or conjugate bases of metal oxide based weak acids.[27,28] These PBA-derived functional materials with hollow/porous structures manifest enhanced properties in energy storage and catalysis.[27–29] However, PBA materials have not been employed as templates to synthesize nanostructured metal sulfides up to now. Thus, it would be of great interest to develop a facile approach to synthesize nanostructured hollow/porous metal sulfides from PBA.

Herein, we present a facile template-engaged approach for the synthesis of cubic nanoframes of metal sulfides via a structure-induced anisotropic chemical etching/anion exchange reaction of PBA nanocubes in the presence of S^{2-} at elevated temperature. We choose NiS as an example to demonstrate the concept in view of the limited success in synthesizing cubic frame-like NiS hollow structures and its widespread applications. An interesting structural evolution process from solid nanocubes to hollow cubic nanoframes is observed. Furthermore, the annealed NiS nanoframes exhibit enhanced electrochemical performance as electrodes for electrochemical capacitors (ECs) and electrocatalysts for hydrogen evolution reaction (HER) in alkaline solution.

We employ a modified precipitation method to synthesize uniform Ni-Co PBA nanocubes,[30] which are then reacted with S^{2-} anions to obtain NiS nanoframes. Panoramic field-emission scanning electron microscopy (FESEM) images show that these PBA nanocubes are highly uniform with an

[*] Dr. X.-Y. Yu, L. Yu, H. B. Wu, Prof. X. W. Lou
School of Chemical and Biomedical Engineering
Nanyang Technological University
62 Nanyang Drive, Singapore 637459 (Singapore)
E-mail: xwlou@ntu.edu.sg
davidlou88@gmail.com
Homepage: http://www.ntu.edu.sg/home/xwlou/
Dr. X.-Y. Yu
Nano-materials and Environment Detection Laboratory, Hefei Institutes of Physical Science, Chinese Academy of Sciences
Hefei 230031 (PR China)

Supporting information for this article is available on the WWW under http://dx.doi.org/10.1002/anie.201500267.

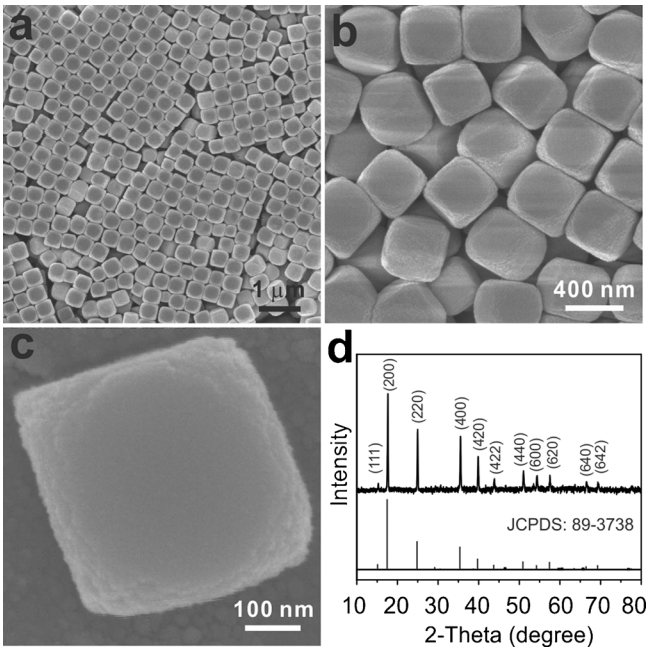

Figure 1. a–c) FESEM images and d) XRD pattern of Ni-Co PB analogue nanocubes with size of 400 nm using nickel nitrate as nickel source.

average size of ca. 400 nm (Figure 1 a). The magnified FESEM images (Figure 1 b,c) reveal that the edges of these nanocubes are rather rough compared to the plane surface. The crystallographic structure and phase purity of the PBA nanocubes are examined by powder X-ray diffraction (XRD). As can be seen from the XRD pattern in Figure 1 d, all of the diffraction peaks could be unambiguously assigned to cubic $Ni_3[Co(CN)_6]_2{\cdot}12\,H_2O$ (JCPDS card no. 89-3738; space group $F\bar{4}3m$, $a=b=c=10.14$ Å, $\alpha=\beta=\gamma=90°$). No additional peaks from impurities are detected, indicating the high purity of the product. The Ni-Co PBA nanocubes then serve as a sacrificial template for the formation of NiS nanoframes. When Ni-Co PBA nanocubes react with an appropriate amount of S^{2-} anions at elevated temperature, the solid nanocubes convert into hollow frame-like particles. FESEM and transmission electron microscopy (TEM) characterizations are carried out to get insight into the nanostructure and morphology of the as-prepared nanoframes. As shown in Figure 2 a,b and Figure S1 (see Supporting Information (SI)), the as-synthesized nanoframes well retain the cubic shape of the PBA precursor particles, while the size has decreased to about 300 nm. An interesting feature of the as-synthesized products is that the six plane surfaces of the cubic structure are completely removed, with only the edges left. A single nanoframe is shown in the magnified FESEM image in Figure 2 c. It is found that the nanoframe with hollow interior is constructed by small nanoparticles. Consistent with FESEM observation, TEM image confirms the frame-like structure of the as-synthesized products (Figure 2 d). Further high-magnification TEM observations reveal the porous structures of these nanoframes (Figure 2 e,f). The thickness of the nanoframes is about 80 to 100 nm (Figure 2 e,f). These nanoframes turn out to be amorphous, with no characteristic peaks in the XRD pattern (Figure S2, see SI). After the controlled annealing treatment at 300 °C in N_2, polycrystalline nanoframes are obtained without apparent change in morphology, as revealed by FESEM examination (Figure S3a, see SI). From the XRD pattern (Figure S2, see SI), the crystallographic phase of the annealed products can be identified as NiS (JCPDS card no. 77-1624), with no additional signals from possible impurities. The lattice fringes in a typical high-resolution TEM image (Figure S3b, see SI) are separated by 0.298 nm, in good agreement with the spacing of (100) planes of NiS. In virtue of the unique hollow frame-like structure and small crystallite size, the annealed NiS nanoframes possess a relatively high Brunauer–Emmett–Teller (BET) surface area of about 143 m^2g^{-1} and a large pore volume of about 0.95 cm^3g^{-1} (Figure S4, see SI) based on measurements of three independent samples. Furthermore, it is found that this strategy can be performed on pre-synthesized Ni-Co PBA nanocubes with different sizes, which offers the feasibility to control the size of the resultant NiS nanoframes. For example, NiS nanoframes with sizes of 100 and 600 nm can be fabricated using the same method by templating against Ni-Co PBA nanocubes with sizes of 200 and 800 nm, respectively (Figure 3). The BET surface area (pore volume) of annealed NiS nanoframes with sizes of 100 and 600 nm is 155 m^2g^{-1} (1.17 cm^3g^{-1}) and 82 m^2g^{-1} (0.71 cm^3g^{-1}) respectively (Figure S5, see SI).

In the present synthesis strategy, precise control over the reaction rate is crucial for producing high-quality NiS nano-

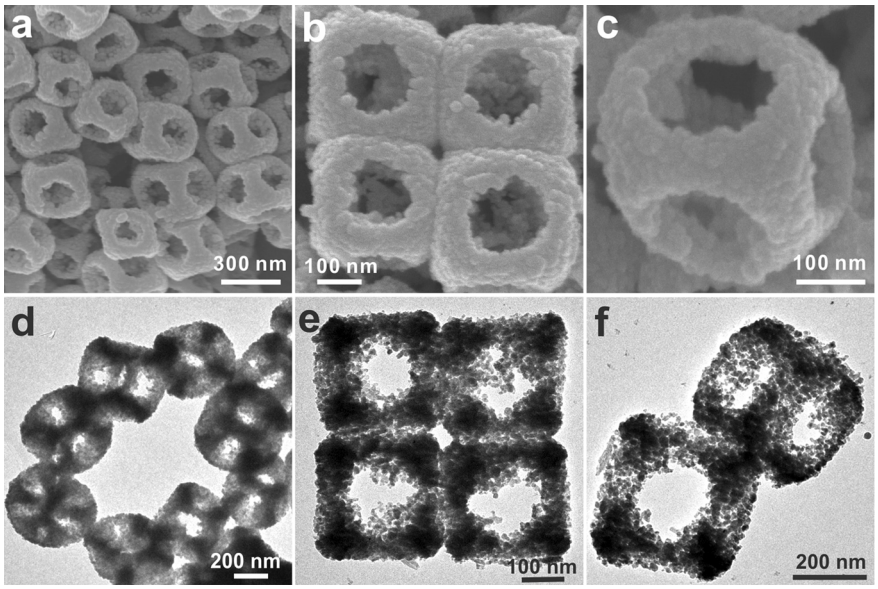

Figure 2. a–c) FESEM and d–f) TEM images of NiS nanoframes with size of 300 nm. 20 mg of Ni-Co PB analogue nanocubes with size of 400 nm react with 40 mg of Na_2S at 100 °C for 6 h.

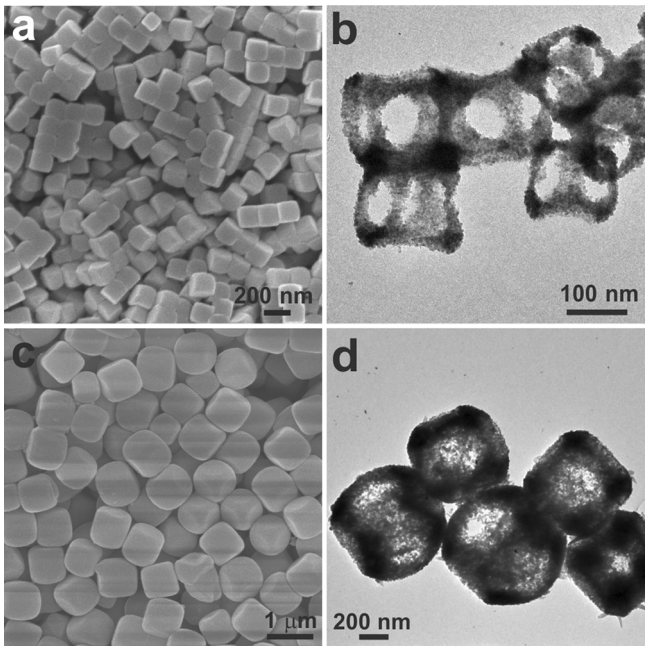

Figure 3. a,c) FESEM images of Ni-Co PB analogue nanocubes with size of 200 nm (a) and 800 nm (c) synthesized using nickel chloride and nickel acetate as nickel source, respectively. b,d) TEM images of NiS nanoframes with size of 100 nm (b) and 600 nm (d). 20 mg of Ni-Co PB analogue nanocubes with size of 200 or 800 nm react with 40 mg of Na_2S at 100 °C for 6 h.

frames. Excessively fast anion exchange will induce severe collapse of the frame-like structures (Figure S6, see SI). Therefore, a proper amount of ethanol is introduced into the reaction system to slow down the anion exchange between $[Co(CN)_6]^{3-}$ and S^{2-}. In addition, high concentration of Na_2S, high reaction temperature, and long reaction time will also lead to collapse of the nanoframes (Figure S6, see SI). At room temperature, it is hard for the Ni-Co PBA nanocubes to evolve into well-defined NiS nanoframes even with high concentration of S^{2-} and prolonged reaction time (Figure S7, see SI). This finding indicates that the structure-induced anisotropic chemical etching/anion exchange between Ni-Co PBA nanocubes and S^{2-} ions is highly dependent on the reaction temperature.

To understand the formation mechanism of the NiS nanoframes, FESEM and energy-dispersive X-ray spectroscopy (EDX) are used to characterize the intermediates collected at different reaction stages. Figure 4a schematically illustrates the interesting morphological evolution of the NiS nanoframes from Ni-Co PBA nanocubes. Based on the FESEM analysis of the samples taken during the reaction process, the morphological change from nanocubes to nanoframes involves several stages, as shown in Figure 4b–e. When the exchange reaction of the Ni-Co PBA nanocubes with S^{2-} ions proceeds for 0.5 h, the edges of the nanocubes are partially etched and become rougher, while their plane surfaces remain unchanged (Figure 4c and Figure S8a, see SI). This observation indicates that the edges of nanocubes with high curvature and probably more defects are more reactive than smooth plane surfaces. When prolonging the reaction duration to 2 h, a unique nanostructure appears (Figure 4d and Figure S8b, see SI). It can be seen that the previous edges have been further etched and converted to a cubic skeleton, while the etching preferentially takes place on the boundary between the skeleton and the rest part, resulting in the contraction of the middle plane surface (Figure 4d). As the reaction continues, the middle plane surface and the core region are completely etched out, and the frame-like structure is finally obtained after reaction for 6 h (Figure 4e). The EDX spectra show the decrease of cobalt content and at the same time the increase of sulfur content as the reaction proceeds, further evidencing the anion exchange between $[Co(CN)_6]^{3-}$ and S^{2-} (Figure S9, see SI).

The formation mechanism of the NiS nanoframes can be explained by a structure-induced anisotropic chemical etching/anion exchange and some mechanism analogous to the nanoscale Kirkendall effect. The edges of Ni-Co PBA nanocubes with high curvature are rougher and expected with more defects compared to the smooth plane surface, which provide more reactive sites for chemical etching/anion exchange. Therefore, the edges are prior etched and subjected to the exchange reaction with S^{2-} ions. A thin shell of NiS is first formed on the edges of Ni-Co PBA nanocubes. At the meantime, as the reaction proceeds, the lateral sides of the less etched plane surface are exposed and become vulnerable to chemical etching. As a result, chemical etching/anion exchange takes place on the lateral face of the less etched middle plane surfaces. According to the Kirkendall effect, the discrepancy of diffusivities of different components in a diffusion couple may lead to the formation of Kirkendall voids close to the interface.[31] In our case, the solid nanocubes are

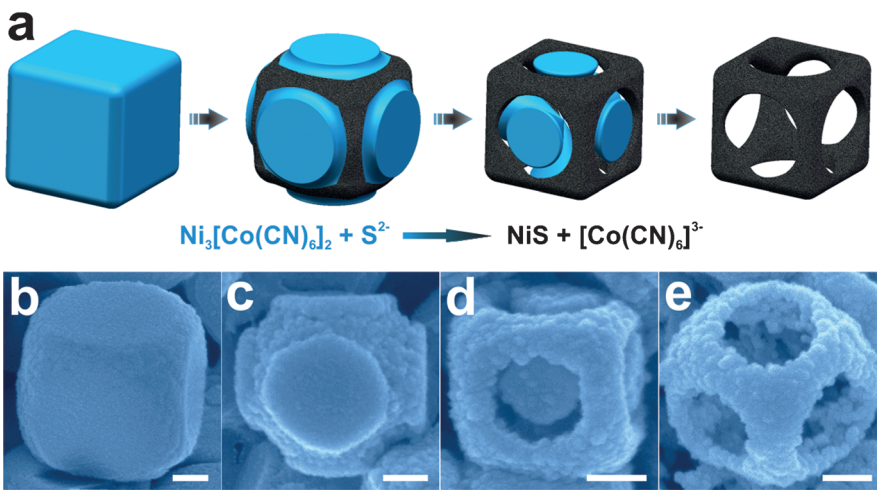

Figure 4. a) Schematic illustration of the formation process of NiS nanoframes. b–e) FESEM images of the products obtained after reaction for b) 0 h, c) 0.5 h, d) 2 h, and e) 6 h. Scale bars: 100 nm. 20 mg of Ni-Co PB analogue nanocubes with size of 400 nm react with 40 mg of Na_2S at 100 °C for different durations.

reacting with Na_2S solution. The continuous outward transport of Ni^{2+} ions and inward transport of S^{2-} ions occur through the formed NiS shell. Due to their larger size, S^{2-} ions diffuse more slowly than Ni^{2+} ions. The unequal diffusion of reacting species (Ni^{2+} and S^{2-} ions) produces voids close to the interface. With the anion exchange reaction going on, the newly formed NiS nuclei would supply the growth of the preformed NiS skeleton on the edges, while the central region of the nanocubes would be completely etched away. These two processes eventually lead to the formation of well-defined NiS nanoframes.

We further investigated the electrochemical properties of the annealed NiS nanoframes with size of 300 nm as electrode materials for ECs in 6 M KOH solution. Figure 5a shows typical cyclic voltammetry (CV) curves of the electrode with a potential window ranging from 0 to 0.55 V vs. a saturated calomel electrode (SCE) at various scanning rates. It can be seen that all of the CV curves exhibit a pair of redox peaks, which are distinct from those of electric doule-layer capacitance, indicating the presence of a reversible Faradic reaction and a pseudocapacitive behavior.[32] With the increase of scanning rate, the current increases accordingly and the shape of the CV curves is maintained, implying a good rate capability. Some typical constant current galvanostatic charge–discharge curves measured at various current densities from 1 to 20 $A g^{-1}$ are shown in Figure 5b. The potential plateaus in the charge–discharge curves are in good agreement with the results of the CV analysis. The average specific capacitance from three samples of NiS nanoframes is calculated from galvonostatic charge/discharge curves and depicted in Figure 5c (note that the capacity in the unit of mAh g^{-1} is also given in the right axis). An average high specific capacitance of 2112 $F g^{-1}$ is obtained at a discharge current density of 1 $A g^{-1}$. At the same current density, the annealed NiS nanoframes with sizes of 100 nm and 600 nm can also deliver high specific capacitance of 2384 $F g^{-1}$ and 1398 $F g^{-1}$, respectively (Figure S10, see SI). The difference in capacitance of NiS nanoframes is probably due to the difference of their specific surface area. At a very high current density of 20 $A g^{-1}$, the NiS nanoframes with size of 300 nm can still deliver an average high specific capacitance of 711 $F g^{-1}$ (Figure 5c). Importantly, the NiS nanoframes electrode shows higher specific capacitance than many of the previous reported nickel sulfides-based electrodes including flaky Ni_3S_2 nanostructures (717 $F g^{-1}$ at 2 $A g^{-1}$),[33] NiS_2 nanocubes (695 $F g^{-1}$ at 1.25 $A g^{-1}$),[34] NiS nanorod/reduced graphene oxide nanocomposites (715.68 $F g^{-1}$ at 1 $A g^{-1}$),[35] NiS microflowers (894.78 $F g^{-1}$ at 1 $A g^{-1}$),[36] and $ZnO@Ni_3S_2$ nanoarray (1529 $F g^{-1}$ at 2 $A g^{-1}$).[37] The cycling performance of the NiS nanoframes with size of 300 nm at a current density of 4 $A g^{-1}$ is shown in Figure 5d. The specific capacitance is 1405 $F g^{-1}$ for the initial cycle, and maintains a high value of 1290 $F g^{-1}$ (91.8% retention) after 4000 cycles. The cycling performance is superior to many other nickel sulfides-based electrode materials.[33,36,37] After cycling, the frame-like structure can be well retained (Figure S11, see SI), demonstrating the structural robustness of these NiS nanoframes.

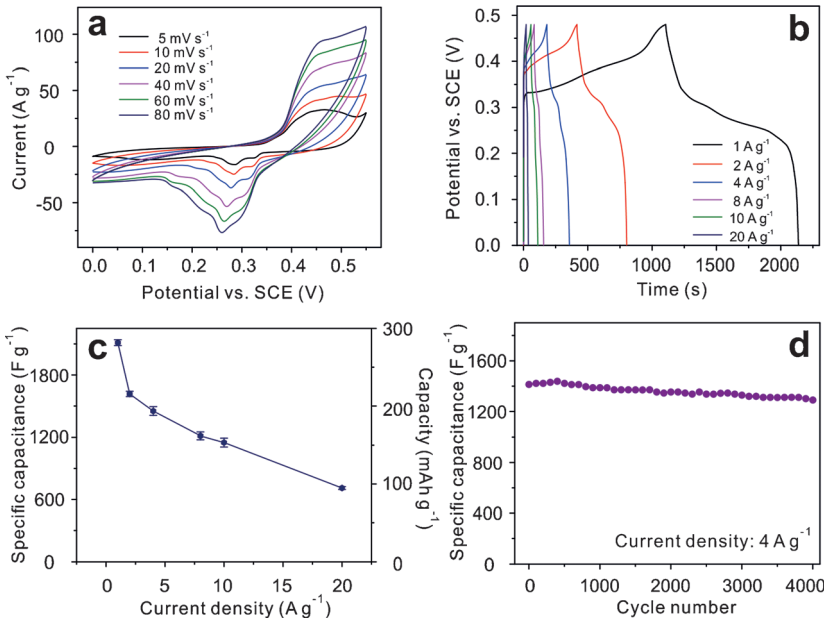

Figure 5. a) Cyclic voltammetry (CV) curves at different scan rates. b) Charge–discharge curves at different current densities, and c) the corresponding specific capacitance calculated from the discharge curves. d) The capacitance cycling performance at a constant current density of 4 $A g^{-1}$. Annealed NiS nanoframes with size of 300 nm are used for capacitive measurements in 6 M KOH solution.

The electrocatalytic activity of the annealed NiS nanoframes for the HER in alkaline electrolyte is also evaluated. Figure S12a (see SI) shows the polarization curves of NiS nanoframes with different size supported on Ni foam and bare Ni foam in 1.0 M KOH with a scan rate of 2 mV s^{-1}. The activity of NiS nanoframes is significantly higher than that of bare Ni foam. Larger cathodic current at the same overpotential is obtained by NiS nanoframes with smaller size and higher specific surface area. Specifically, the NiS nanoframes with size of 100 nm only need an overpotential of 94 mV to drive a current density of 10 mA cm^{-2}, while the overpotential required for NiS nanoframes with size of 300 and 600 nm to achieve the current density is 115 and 148 mV, respectively. Additionally, from the Tafel plots (Figure S12b, see SI) one can see that all samples of NiS nanoframes exhibit smaller Tafel slopes than bare Ni foam, demonstrating relatively good electrochemical reaction kinetics. The calculated exchange current densities (rate constants) of various samples at $\eta = 0$ by the extrapolation method are 0.17, 2.2, 1.3, and 1 μA cm^{-2} for Ni foam, NiS nanoframes (100 nm), NiS nanoframes (300 nm), and NiS nanoframes (600 nm), respectively. This further demonstrates that the smaller NiS nanoframes exhibit higher electrocatalytic activity. The HER activity of NiS nanoframe is better than that of the reported Ni_3S_2 nanoparticles or Ni_3S_2/carbon

nanotube nanocomposites in alkaline electrolyte.[38] Additionally, the stability of the NiS nanoframes catalyst with size of 300 nm is evaluated by chronoamperometry measurement at a constant potential of −0.115 V vs. reversible hydrogen electrode (RHE) in 1.0 M KOH and the current–time plot is presented in Figure S12c (see SI). The stable current over 16 h of continuous operation, which only decreases by about 8%, suggests that the NiS nanoframe electrode exhibits good durability for HER.

The remarkable pseudocapacitive and HER performance is probably related to the unique nanostructure of these NiS nanoframes. To be specific, the 3D frame-like hollow and porous structure with high surface-area-to-volume ratio endows a large electrode–electrolyte contact area. The small nanoparticles as building blocks possess large electrochemically active surface area for electrochemical reactions. Meanwhile, the robust structure of the NiS nanoframes might also grant high stability for the electrochemical applications.

In summary, we have demonstrated a novel template-engaged structure-induced anisotropic chemical etching/anion exchange strategy for the synthesis of cubic NiS nanoframes by anion exchange of Ni-Co PB analogue nanocubes with S^{2-} ions. The precursor nanocubes undergo a very unusual structural evolution process and transform into a frame-like nanostructure, which originates from the different reactivity between the edge and plane surface of the precursor nanocubes. Moreover, the present strategy can be applied to Ni-Co PB analogue nanocube templates with different sizes, which enables the synthesis of NiS nanoframes with controllable dimension. This strategy might open up a new way to synthesize a variety of nanoframe-like hollow structures. When evaluated for electrochemical applications, the NiS nanoframes exhibit enhanced capacitive performance for electrochemical capacitors and electrocatalytic activity for hydrogen evolution reaction.

Keywords: ion exchange · metal–organic frameworks · nanoframes · nanostructures · nickel sulfide

How to cite: *Angew. Chem. Int. Ed.* **2015**, *54*, 5331–5335
Angew. Chem. **2015**, *127*, 5421–5425

[1] F. Caruso, R. A. Caruso, H. Möhwald, *Science* **1998**, *282*, 1111–1114.
[2] X. W. Lou, L. A. Archer, Z. C. Yang, *Adv. Mater.* **2008**, *20*, 3987–4019.
[3] X. Y. Lai, J. E. Halpert, D. Wang, *Energy Environ. Sci.* **2012**, *5*, 9944–9944.
[4] J. B. Joo, Q. Zhang, M. Dahl, I. Lee, J. Goebl, F. Zaera, Y. D. Yin, *Energy Environ. Sci.* **2012**, *5*, 6321–6327.
[5] J. Hu, M. Chen, X. S. Fang, L. W. Wu, *Chem. Soc. Rev.* **2011**, *40*, 5472–5491.
[6] J. Y. Wang, N. L. Yang, H. J. Tang, Z. H. Dong, Q. Jin, M. Yang, D. Kisailus, H. J. Zhao, Z. Y. Tang, D. Wang, *Angew. Chem. Int. Ed.* **2013**, *52*, 6417–6420; *Angew. Chem.* **2013**, *125*, 6545–6548.
[7] X. Wang, H. B. Fu, A. D. Peng, T. Y. Zhai, Y. Ma, F. L. Yuan, J. N. Yao, *Adv. Mater.* **2009**, *21*, 1636–1640.
[8] E. Gonzalez, J. Arbiol, V. F. Puntes, *Science* **2011**, *334*, 1377–1380.
[9] Y. E. Wu, D. S. Wang, G. Zhou, R. Yu, C. Chen, Y. D. Li, *J. Am. Chem. Soc.* **2014**, *136*, 11594–11597.
[10] X. Hong, D. S. Wang, S. F. Cai, H. P. Rong, Y. D. Li, *J. Am. Chem. Soc.* **2012**, *134*, 18165–18168.
[11] B. Y. Xia, H. B. Wu, X. Wang, X. W. Lou, *J. Am. Chem. Soc.* **2012**, *134*, 13934–13937.
[12] X. Wu, Y. F. Yu, Y. Liu, Y. Xu, C. B. Liu, B. Zhang, *Angew. Chem. Int. Ed.* **2012**, *51*, 3211–3215; *Angew. Chem.* **2012**, *124*, 3265–3269.
[13] Z. Y. Wei, H. Matsui, *Nat. Commun.* **2014**, *5*, 3870.
[14] D. Kim, J. Park, K. An, N. K. Yang, J. G. Park, T. Hyeon, *J. Am. Chem. Soc.* **2007**, *129*, 5812–5813.
[15] S. F. Xie, N. Lu, Z. X. Xie, J. G. Wang, M. J. Kim, Y. N. Xia, *Angew. Chem. Int. Ed.* **2012**, *51*, 10266–10270; *Angew. Chem.* **2012**, *124*, 10412–10416.
[16] X. M. Lu, L. Au, J. McLellan, Z. Y. Li, M. Marquez, Y. N. Xia, *Nano Lett.* **2007**, *7*, 1764–1769.
[17] C. H. Kuo, M. H. Huang, *J. Am. Chem. Soc.* **2008**, *130*, 12815–12820.
[18] M. A. Mahmoud, M. A. El-Sayed, *J. Am. Chem. Soc.* **2010**, *132*, 12704–12710.
[19] C. Chen, Y. J. Kang, Z. Y. Huo, Z. W. Zhu, W. Y. Huang, H. L. L. Xin, J. D. Snyder, D. G. Li, J. A. Herron, M. Mavrikakis, M. F. Chi, K. L. More, Y. D. Li, N. M. Markovic, G. A. Somorjai, P. D. Yang, V. R. Stamenkovic, *Science* **2014**, *343*, 1339–1343.
[20] Y. M. Sui, W. Y. Fu, Y. Zeng, H. B. Yang, Y. Y. Zhang, H. Chen, Y. X. Li, M. H. Li, G. T. Zou, *Angew. Chem. Int. Ed.* **2010**, *49*, 4282–4285; *Angew. Chem.* **2010**, *122*, 4378–4381.
[21] L. Hu, Q. W. Chen, *Nanoscale* **2014**, *6*, 1236–1257.
[22] M. Hu, A. A. Belik, M. Imura, Y. Yamauchi, *J. Am. Chem. Soc.* **2013**, *135*, 384–391.
[23] M. Hu, S. Furukawa, R. Ohtani, H. Sukegawa, Y. Nemoto, J. Reboul, S. Kitagawa, Y. Yamauchi, *Angew. Chem. Int. Ed.* **2012**, *51*, 984–988; *Angew. Chem.* **2012**, *124*, 1008–1012.
[24] L. Hu, N. Yan, Q. W. Chen, P. Zhang, H. Zhong, X. R. Zheng, Y. Li, X. Y. Hu, *Chem. Eur. J.* **2012**, *18*, 8971–8977.
[25] L. Hu, P. Zhang, H. Zhong, X. R. Zheng, N. Yan, Q. W. Chen, *Chem. Eur. J.* **2012**, *18*, 15049–15056.
[26] M. Hu, A. A. Belik, M. Imura, K. Mibu, Y. Tsujimoto, Y. Yamauchi, *Chem. Mater.* **2012**, *24*, 2698–2707.
[27] L. Zhang, H. B. Wu, X. W. Lou, *J. Am. Chem. Soc.* **2013**, *135*, 10664–10672.
[28] L. Zhang, H. B. Wu, S. Madhavi, H. H. Hng, X. W. Lou, *J. Am. Chem. Soc.* **2012**, *134*, 17388–17391.
[29] L. Zhang, L. Y. Shi, L. Huang, J. P. Zhang, R. H. Gao, D. S. Zhang, *ACS Catal.* **2014**, *4*, 1753–1763.
[30] M. Hu, S. Ishihara, K. Ariga, M. Imura, Y. Yamauchi, *Chem. Eur. J.* **2013**, *19*, 1882–1885.
[31] M. Wirtz, C. R. Martin, *Adv. Mater.* **2003**, *15*, 455–458.
[32] W. J. Zhou, X. H. Cao, Z. Y. Zeng, W. H. Shi, Y. Y. Zhu, Q. Y. Yan, H. Liu, J. Y. Wang, H. Zhang, *Energy Environ. Sci.* **2013**, *6*, 2216–2221.
[33] S. W. Chou, J. Y. Lin, *J. Electrochem. Soc.* **2013**, *160*, D178–D182.
[34] H. Pang, C. Z. Wei, X. X. Li, G. C. Li, Y. H. Ma, S. J. Li, J. Chen, J. S. Zhang, *Sci. Rep.* **2014**, *4*, 3577.
[35] J. Q. Yang, X. C. Duan, W. Guo, D. Li, H. L. Zhang, W. J. Zheng, *Nano Energy* **2014**, *5*, 74–81.
[36] J. Q. Yang, X. C. Duan, Q. Qin, W. J. Zheng, *J. Mater. Chem. A* **2013**, *1*, 7880–7884.
[37] Z. C. Xing, Q. X. Chu, X. B. Ren, C. J. Ge, A. H. Qusti, A. M. Asiri, A. O. Al-Youbi, X. P. Sun, *J. Power Sources* **2014**, *245*, 463–467.
[38] T. W. Lin, C. J. Liu, C. S. Dai, *Appl. Catal. B* **2014**, *154*, 213–220.

Received: January 12, 2015
Revised: February 4, 2015
Published online: February 20, 2015

